Aging Cell (2011) **10,** pp292–304 Doi: 10.1111/j.1474-9726.2010.00666.x

Age-associated increase in heterochromatic marks in murine and primate tissues

Jill A. Kreiling,[1] Mimi Tamamori-Adachi,[1,2] Alec N. Sexton,[1,*] Jessie C. Jeyapalan,[1] Ursula Munoz-Najar,[1] Abigail L. Peterson,[1] Jayameenakshi Manivannan,[1] Elizabeth S. Rogers,[1] Nikolay A. Pchelintsev,[3] Peter D. Adams[3] and John M. Sedivy[1]

[1]Department of Molecular Biology, Cell Biology and Biochemistry, Brown University, Providence, RI 02903, USA
[2]Department of Biochemistry, Teikyo University School of Medicine, Tokyo 173-8605, Japan
[3]CRUK Beatson Labs, University of Glasgow, Glasgow G61 1BD, UK

Summary

Chromatin is highly dynamic and subject to extensive remodeling under many physiologic conditions. Changes in chromatin that occur during the aging process are poorly documented and understood in higher organisms, such as mammals. We developed an immunofluorescence assay to quantitatively detect, at the single cell level, changes in the nuclear content of chromatin-associated proteins. We found increased levels of the heterochromatin-associated proteins histone macro H2A (mH2A) and heterochromatin protein 1 beta (HP1β) in human fibroblasts during replicative senescence in culture, and for the first time, an age-associated increase in these heterochromatin marks in several tissues of mice and primates. Mouse lung was characterized by monophasic mH2A expression histograms at both ages, and an increase in mean staining intensity at old age. In the mouse liver, we observed increased age-associated localization of mH2A to regions of pericentromeric heterochromatin. In the skeletal muscle, we found two populations of cells with either low or high mH2A levels. This pattern of expression was similar in mouse and baboon, and showed a clear increase in the proportion of nuclei with high mH2A levels in older animals. The frequencies of cells displaying evidence of increased heterochromatinization are too high to be readily accounted for by replicative or oncogene-induced cellular senescence, and are prominently found in terminally differentiated, postmitotic tissues that are not conventionally thought to be susceptible to senescence. Our findings distinguish specific chromatin states in individual cells of mammalian tissues, and provide a foundation to investigate further the progressive epigenetic changes that occur during aging.

Key words: aging; cellular senescence; epigenetics; heterochromatin; immunofluorescence.

Introduction

Functional decline of biologic structures that are inherently difficult to maintain is an important aspect of aging. Chromatin may be one such structure (Oberdoerffer & Sinclair, 2007), and it is rapidly becoming apparent that it may be subject to extensive age-associated remodeling (Fraga *et al.*, 2005; Sedivy *et al.*, 2008).

Chromatin is broadly divided into euchromatin and heterochromatin. Euchromatin is decondensed during interphase and permissive for transcription. Heterochromatin is significantly more compacted and inhibits transcription, and can be further subdivided into two types, constitutive and facultative. The former is found at a variety of repetitive elements, such as centromeres, telomeres, and interspersed retrotransposons, and until recently was believed to remain relatively constant. Facultative heterochromatin is typically established during regulated cell differentiation processes, such as X chromosome silencing in female cells, or repression of homeobox genes by the polycomb group (PcG) proteins during embryogenesis (Simon & Kingston, 2009).

Chromatin is a highly dynamic entity. Heterochromatin can spread along chromosomes, but this can also be reversed allowing the re-expression of silenced genes (Talbert & Henikoff, 2006; Berger, 2007; Grewal & Jia, 2007). Global decreases in DNA methylation have been documented in aging cells and organisms (Wilson *et al.*, 1987; Sedivy *et al.*, 2008; Calvanese *et al.*, 2009). Closer scrutiny reveals complex changes occurring in multiple dimensions. For example, overall DNA methylation decreases, and this occurs predominantly in repetitive DNA regions (Bollati *et al.*, 2009; Bork *et al.*, 2010; Jintaridth & Mutirangura, 2010), while increased methylation occurs at certain CpG islands (Rakyan *et al.*, 2010; Teschendorff *et al.*, 2010), perhaps resulting in the repression of some nearby genes. Furthermore, specific pathways such

Correspondence
John M. Sedivy, Department of Molecular Biology, Cell Biology and Biochemistry, Laboratories for Molecular Medicine, 70 Ship Street, Providence, RI 02903, USA. Tel.: +401 863 7631; fax: +401 863 9653;
e-mail: john_sedivy@brown.edu
Or
Jill A. Kreiling, Department of Molecular Biology, Cell Biology and Biochemistry, Laboratories for Molecular Medicine, 70 Ship Street, Providence, RI 02903, USA. Tel.: +401 863-7674; fax: +401 863 9653;
e-mail: jill_kreiling@brown.edu
*Present address: Alec N. Sexton, Department of Molecular and Cell Biology, University of California, Berkeley, CA 94720-3200, USA.

Accepted for publication *19 November 2010*

Aging Cell

as PcG show relaxation, allowing increased expression of genes under its regulation. In other cases, complex redistributions have been seen, such as the movement of the yeast SIR2 histone deacetylase to telomeres, or its mammalian homolog SIRT1 to sites of DNA damage (Kennedy *et al.*, 1997; Oberdoerffer *et al.*, 2008).

Replicative cellular senescence was first described as an irreversible growth arrest triggered by the accumulation of a discrete number of cell divisions (Hayflick & Moorhead, 1961). The underlying cause of senescence due to replicative exhaustion is telomere shortening (Bodnar *et al.*, 1998; Wright & Shay, 2002). However, replicative senescence is in fact a collection of interrelated states that can be triggered by distinct intrinsic and extrinsic stresses including irradiation, reactive oxygen species, and even nutrient imbalances (Sedivy *et al.*, 2007; Adams, 2009). Recent work has implicated oncogene-induced cellular senescence (OIS) as an important *in vivo* tumor suppressor mechanism (Collado *et al.*, 2007; Prieur & Peeper, 2008).

A terminal step of senescence frequently induced by telomere exhaustion, oncogenes, and genotoxic stress is extensive heterochromatinization and formation of nuclear structures designated senescence-associated heterochromatin foci (SAHF) (Narita *et al.*, 2003). SAHF contain heterochromatin protein 1 (HP1), the histone variant macro H2A (mH2A) and repressive histone marks such as histone H3 trimethylated on lysine 9 (H3K9Me3). SAHF formation is mediated by the p16-pRb pathway in response to upstream signals and involves histone chaperones and other assembly factors (Zhang *et al.*, 2005, 2007). Interestingly, histone H1 is depleted from SAHF and replaced with high mobility group A (HMGA) proteins (Funayama *et al.*, 2006; Narita *et al.*, 2006). Although the heterochromatinization appears to involve entire chromosomes, many regions escape and have been proposed to be arranged as loops that emanate from the SAHF.

The considerable amount of research on SAHF has focused on OIS using normal human diploid fibroblasts (HDF) or other cell culture models, but whether SAHF form in an organismal context remains unknown. Given our increasing realization of the probable importance of epigenetic changes in aging, this is a question of considerable interest. We previously developed an assay that can score, at the single-cell level, the occurrence of telomere-dependent senescence (TDS) in tissue biopsies (Herbig *et al.*, 2004, 2006). We are particularly interested in single cell assays because our work, as well as other studies on single cells (Bahar *et al.*, 2006), indicate that aging tissues are mosaics of normal cells with interspersed senescent (or otherwise age-compromised) cells. Furthermore, senescent cells are likely to be differentially represented among morphologic structures, different cell types, or regions of pathology within tissues. In this communication, we report the development of an assay to score quantitatively the heterochromatin content of single nuclei, and apply these methods to investigate aging in murine and primate tissues.

Results

Expression of heterochromatic marks in cultured fibroblasts

Senescence-associated heterochromatin foci were initially reported as regions of high intensity staining with general DNA dyes such as DAPI, and subsequently as foci of immunofluorescent staining with a variety of antibodies against components or marks of heterochromatin, such as HP1α, β or γ, mH2A, H3K9Me2, etc. (Narita *et al.*, 2003; Zhang *et al.*, 2005; Funayama *et al.*, 2006). While OIS typically elicits pronounced SAHF, the extent of their formation can vary considerably depending on the oncogene or the strain of HDF used. SAHF formation during TDS is even more uneven, with the BJ strain demonstrating no SAHF at all, while other strains such as IMR90 or WI38 display varying levels of SAHF (Narita *et al.*, 2003). The strain used in our laboratory, LF1, does display SAHF, but even completely senescent cultures contain considerable numbers of cells without SAHF.

Careful examination of several human, primate, and murine tissues failed to demonstrate SAHF-like foci; however, we noted cell-to-cell variability in the intensity of the signals produced by several heterochromatin-directed antibodies. We therefore turned our attention to quantify the absolute levels of the signals, rather than visualizing discrete morphologic structures like SAHF. An important breakthrough came when we realized that for abundant proteins, such as chromatin components, recommended antibody dilutions are not in the linear response range. It is first necessary to titrate the antibody concentration such that using either more antibody or longer incubation times do not result in increased signal. At this point, the antigenic binding sites are saturated and the assay can accurately quantify the amount of target protein present in individual nuclei. This titration process (Fig. S1) must be repeated for each target protein or antibody to ensure that the assay is run under conditions of probe (antibody) excess. These saturating concentrations were found to be at least tenfold higher (Table S1) than typically recommended in standard immunofluorescence assays.

Images acquired under these conditions for mH2A and HP1β (Fig. 1), two known components of SAHF, showed a clear passage-associated increase in nuclear staining intensity. The increased levels were already apparent in late passage cultures well before the complete cessation of proliferation. No increase was seen in early passage cells rendered quiescent by contact inhibition and serum deprivation, indicating that the effect is not a general consequence of cell cycle arrest.

Based on these preliminary data, we developed a single-cell assay capable of quantitatively scoring the expression levels of nuclear proteins of interest in microscopic images: (i) cells are stained with primary and secondary antibodies, and with DAPI, at predetermined saturating concentrations; (ii) images are acquired within the linear range for all fluorophores; (iii) a region of interest (ROI) is drawn around each nucleus in the DAPI channel using appropriate software; (iv) the ROI is transferred to the

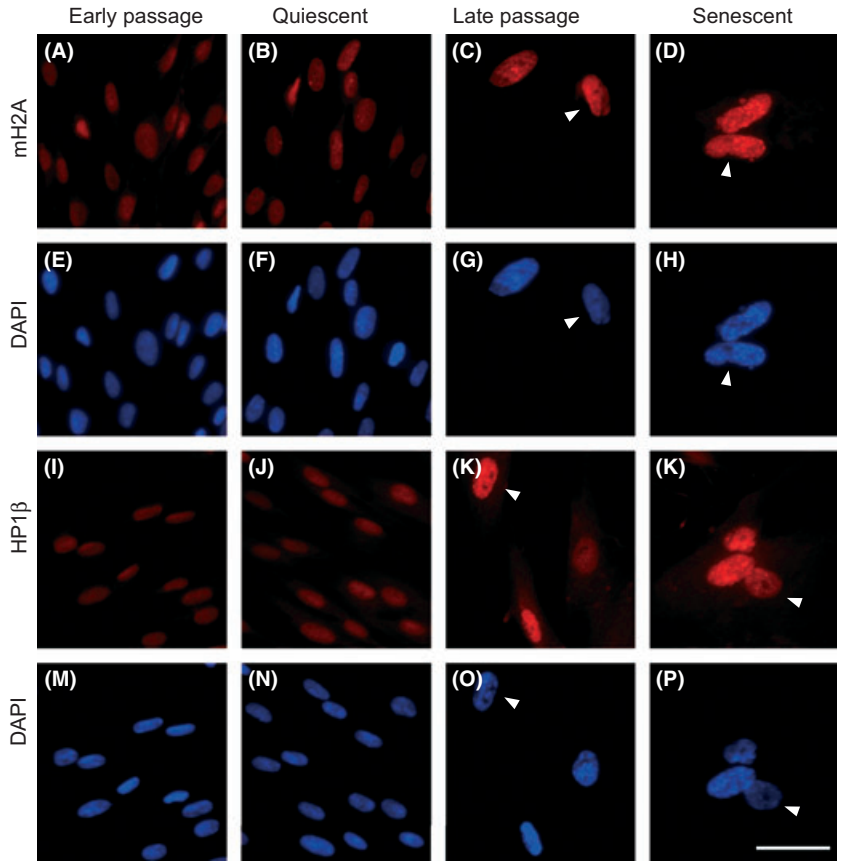

Fig. 1 Representative immunofluorescent images of histone macroH2A (mH2A) and heterochromatin protein 1 beta (HP1β) protein expression in the nuclei of human fibroblasts at different replicative ages. LF1 cells were stained and images acquired as described in Experimental procedures. The mH2A antibody was directly conjugated to Alexa Fluor 647. HP1β was visualized using a secondary antibody conjugated to Cy3. Early passage: vigorously growing cultures within the first third of their replicative lifespan. Quiescent: early passage cells were contact inhibited and then cultured in 0.25% serum for 48 h. Late passage: cultures within 8–12 population doublings of their terminal senescent arrest. Senescent: cultures whose cell numbers have not increased for a minimum of 2 weeks. Flow cytometric cell cycle profiles for early passage, quiescent and senescent cultures are shown in Fig. S2. Arrowheads indicate the variety of senescence-associated heterochromatin foci morphologies seen in LF1 cells: cell showing robust mH2A and DAPI foci, panels D, H; cell showing intermediate but poorly resolved HP1β and DAPI foci, panels K, O; cell showing very few and small HP1β foci and no DAPI foci, panels L, P; cell showing no mH2A or DAPI foci but high overall levels of mH2A, panels C, G.

other channels and signal intensities are computed within them. The assay can be further streamlined by directly conjugating the primary antibody with a fluorophore, and by using lenses with large depths of focus to capture most of the light in a single image focused at the center of a nucleus. The data can be conveniently displayed as histograms of cell (nuclei) numbers against fluorescence intensity (Fig. 2A) according to the convention of one-dimensional flow cytometry.

As SAHF have been found to be enriched for both mH2A and HP1β and the two proteins colocalize (Zhang *et al.*, 2005), we examined to what extent their increased nuclear content in senescent cells is correlated in individual cells (Fig. 2B). Double staining of cultures with antibodies against both mH2A and HP1β showed a high level of correlation at the single-cell level at all replicative ages.

The increases in mH2A and HP1β levels seen by microscopy (Fig. 2) were further investigated using immunoblotting (Fig. 3). Normalization of immunoblotting data from senescent cells is complicated by the well-known fact that the cells increase significantly in size, including protein content (Cristofalo & Pignolo, 1993). We verified this and found that our late passage cells contained three- to fivefold more total protein than early passage cells. We used protocols that allow the measurement of total protein and DNA in the same extracts, and subsequently immunoblotted the extracts for core histones such as H2B or H3. We found that cell number, DNA content, and H2B or H3 expression were very closely correlated and constant across all replicative ages. For the immunoblotting analysis of mH2A and HP1β, we therefore loaded equivalent numbers of cells in each lane and further normalized the data internally to H2B (Fig. 3). We found that the mH2A expression was increased threefold in late passage cells and HP1β was increased twofold. Both results were statistically significant across three separate experiments and correlate well with the increases observed with the microscopic assay. In contrast, only minimal changes in mH2A or HP1β mRNA levels were seen under any condition (Fig. S3).

Senescence-associated β-galactosidase (SA-β-Gal) (Dimri *et al.*, 1995) and SAHF, visualized either as DAPI or mH2A foci,

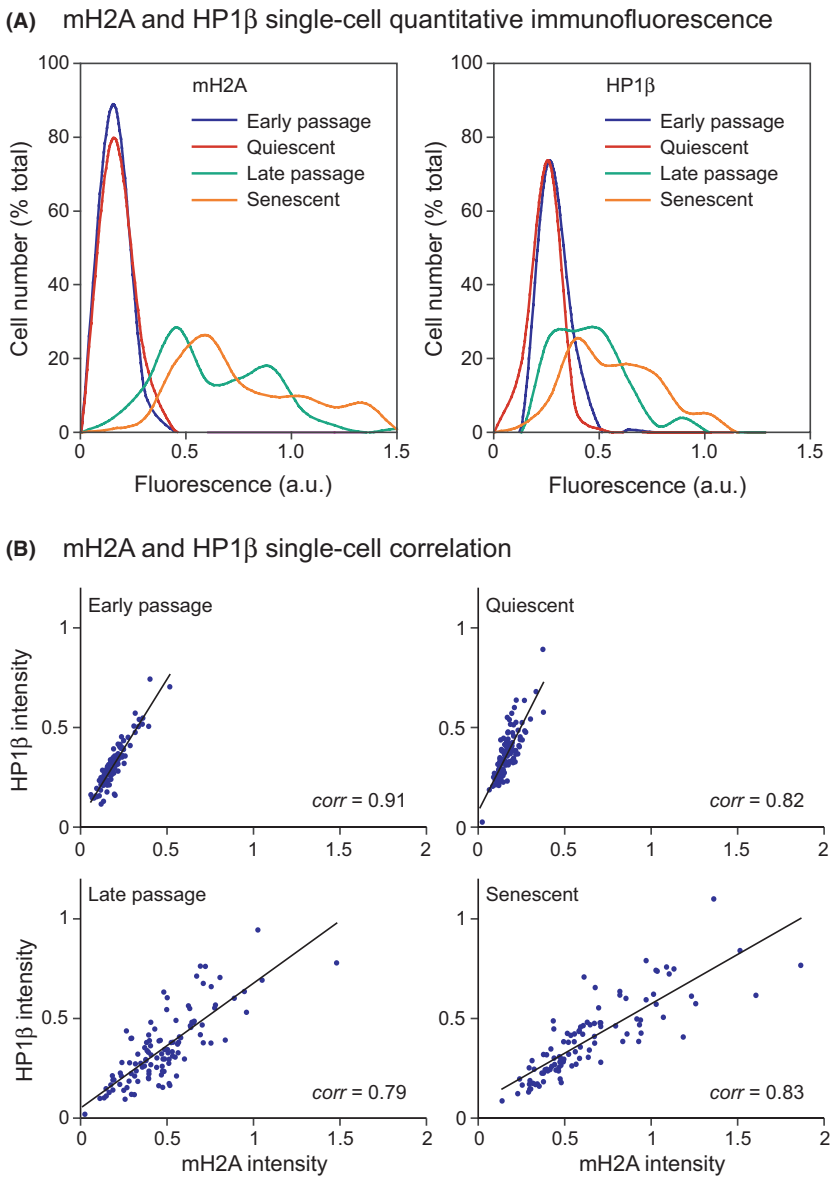

Fig. 2 Quantitative measurements of histone macroH2A (mH2A) and heterochromatin protein 1 beta (HP1β) protein levels in human fibroblasts at different replicative ages. (A) Immunofluorescent images (illustrated in Fig. 1) were quantified as indicated in Experimental procedures and plotted as histograms of cell number (% of total) against fluorescence intensity in arbitrary units (a.u.). mH2A, left panel; HP1β, right panel. Replicative ages of the cultures were as indicated in Fig. 1. A minimum of 100 cells were scored for each age group. (B) Cells were co-stained with mH2A and HP1β antibodies, images were acquired, and individual cells were scored in three channels (using the DAPI, rhodamine and Cy5 filter sets for the nuclei, HP1β and the mH2A, respectively). Data are plotted as 2-D scatter plots of mH2A and HP1β intensities.

appear with essentially the same kinetics as WI38 cells approach and enter senescence (Zhang *et al.*, 2005). We observed the same relationship in LF1 HDF using the quantitative mH2A assay (data not shown). For technical reasons, we have been unable to combine the immunofluorescence mH2A assay with either the SA-β-Gal assay or the telomere dysfunction-induced foci (TIF) assay (Herbig *et al.*, 2004) for multiparameter staining of the same samples. We have shown previously that p16 and p21 appear to be upregulated independently as HDF cultures approach senescence (Herbig *et al.*, 2004). We have also observed no correlation between the upregulation of γH2AX or 53BP1 and p16, but we did observe a correlation between the upregulation of mH2A and p16 (data not shown). These data are consistent with γH2AX, 53BP1, and p21 being in one pathway, and with HIRA, mH2A, and p16 being in a distinct pathway. It should be noted that these correlations are only relevant in cultures approaching senescence that still contain significant numbers of replicating cells, because cells that have become fully senescent are uniformly positive for all the aforementioned markers.

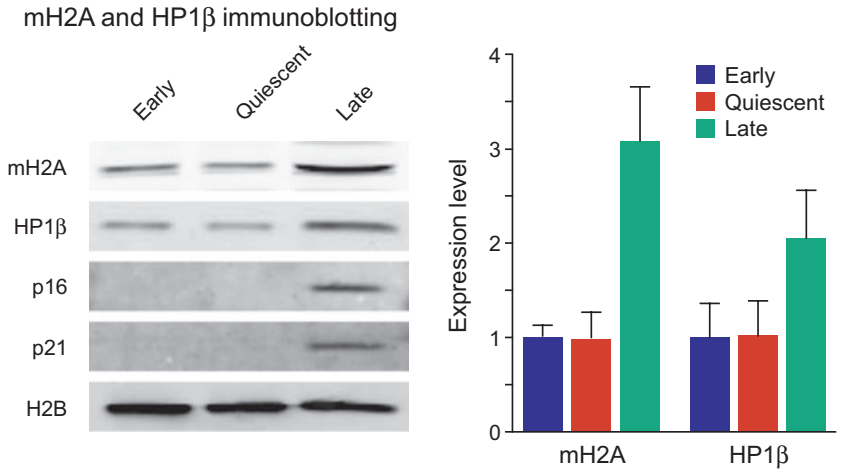

Fig. 3 Immunoblotting analysis of total cellular extracts. Left panel: representative images from one experiment. Lanes were loaded for equivalent cell numbers. Note the clear upregulation of the cyclin-dependent kinase inhibitors p16 and p21 in late passage cells, indicative of entry into cellular senescence. Right panel: immunoblots were quantified using the LI-COR Odyssey infrared imaging system. Histone macroH2A (mH2A) and heterochromatin protein 1 beta (HP1β) levels were normalized to H2B levels detected in the same lane and are expressed as a ratio of mH2A or HP1β to H2B a.u. The values shown are the mean of three separate experiments. Error bars indicate the SEM. The differences in expression between early and late cells are significant at $P = 0.0032$ and $P = 0.042$ for mH2A and HP1β, respectively, calculated using a two-tailed student's test.

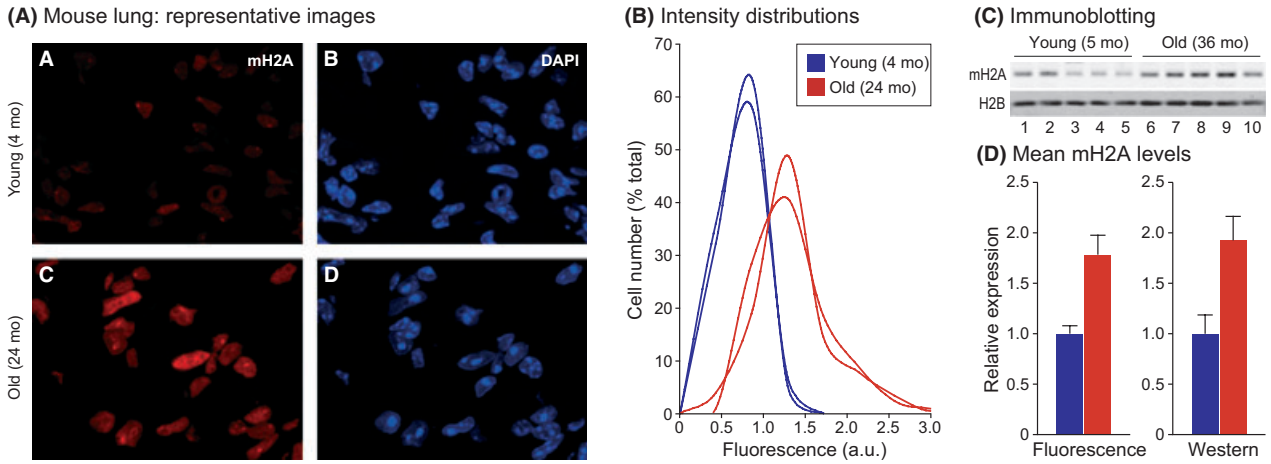

Fig. 4 Quantitative measurements of histone macroH2A (mH2A) protein levels in mouse lung. (A) Representative images of sections from 4- and 24-month-old female lung. The bright foci in the DAPI images are the prominent pericentromeric heterochromatin found in this species. (B) Immunofluorescent images collected in the experiment shown in panel A were quantified as indicated in Experimental procedures, expressed as ratios of mH2A and DAPI intensities for each nucleus, and plotted as histograms of cell number (% of total) against fluorescence intensity in arbitrary units (a.u.). Representative histograms for two young (blue) and two old (red) animals are shown. (C) Immunoblotting analysis of total tissue extracts from 5- and 36-month-old male lungs. Five young animals (lanes 1–5) and five old animals (lanes 6–10) were included in the analysis. Lanes were loaded for equivalent DNA content and blots were probed with mH2A and H2B antibodies. (D) Quantification and comparison of mH2A levels detected by immunofluorescence and immunoblotting. Left panel: average intensities of each histogram from the experiment shown in panel B were computed, and mean values were calculated for the young (blue) and old (red) age groups. A total of four young and six old animals were included in the analysis. The mH2A level for the young age group was set to 1. Error bars indicate the SEM. The difference in mH2A levels between the young and old groups is significant at $P = 0.0094$ calculated using a two-tailed student's test. Right panel: immunoblots from the experiment shown in panel C were quantified using the LI-COR Odyssey infrared imaging system. mH2A levels were normalized to H2B levels detected in the same lane. A total of five young and five old animals were included in the analysis. The mH2A level for the young age group was set to 1. Error bars indicate the SEM. The difference in mH2A levels between the young and old groups is significant at $P = 0.0086$ calculated using a two-tailed student's test. All experiments were repeated at least twice with consistent results.

Expression of heterochromatic marks in murine tissues

Having demonstrated the efficacy and sensitivity of the single cell immunofluorescence assay in cultured cells, we asked whether changes in chromatin states also occur as a function of age *in vivo*. To improve further the assay, we made several changes: (i) use confocal microscopy to collect a z-series encompassing the full thickness of the tissue for each field; (ii) apply 3-D image reconstruction to compute average intensities for the entire volume of each nucleus; and (iii) normalize mH2A intensities to DAPI intensities for each nucleus.

Elevated levels of mH2A were readily apparent in lung nuclei of 24-month-old C57BL/6 females (Fig. 4A). Quantification of the imaging data revealed histograms that were typically quite symmetrical in young animals (Fig. 4B). In old animals, the histograms were broadened, shifted to higher intensities, and often displayed high intensity shoulders. Immunoblotting analysis of total lung tissue extracts confirmed the age-associated increase in mH2A levels (Fig. 4C). While some heterogeneity was seen between individual animals, the mean levels of mH2A calculated for groups of five young (5 months) and old (36 months) male animals showed a highly significant 1.9-fold increase in the old group (Fig. 4D). The correlation between the fold-change increase observed by the immunoblotting and that by immunofluorescence methods was excellent (Fig. 4D). Examination of additional samples from 27-month-old males confirmed that the increase in mH2A levels affects animals near their median lifespan as well as very old animals of both sexes. Finally, using HP1β antibody in the immunofluorescence and immunoblotting assays showed the same trends and patterns for this antigen as seen with mH2A.

Examination of liver tissue showed that the total mH2A intensity increased with age; however, because of a significant increase in the size and volume of the liver nuclei in old animals (due to the age-associated polyploidization seen in this tissue), the normalized mH2A intensity did not increase significantly. Likewise, mH2A levels did not increase when assessed by immunoblotting and normalized to either DNA or H2B.

We did, however, observe a significant redistribution of mH2A within the nuclei of old animals (Fig 5A). Mouse genomes contain distinct regions of DNA repeats known as γ-satellites that surround the centromeres and condense into pericentromeric heterochromatin foci (Vissel & Choo, 1989). Liver nuclei show particularly prominent pericentromeric heterochromatin foci that are readily seen with simple DAPI staining in both young and old animals. However, while young nuclei stain relatively uniformly with mH2A, old nuclei typically display prominent mH2A foci that colocalize with the DAPI foci. The pericentromeric localization of the mH2A foci was verified using a human anti-centromere autoantibody.

Examination of lung nuclei, which are smaller and do not undergo polyploidization, revealed the same phenomenon (Fig. 5B). In both lung and liver, approximately 30% of nuclei had at least one mH2A-positive pericentromeric focus in young animals, while the number of nuclei containing mH2A-positive foci doubled in older animals (Fig. 5C). Thus, in addition to an overall increase in mH2A levels in certain tissues, mH2A can also undergo a profound age-associated redistribution. Our data are indicative of increasing concentrations of mH2A in regions of constitutive heterochromatin; whether more subtle or specific movements can occur remains to be investigated with higher resolution methods.

Age-associated increases in mH2A levels were also readily apparent in the skeletal muscle (Fig. 6A). In this case, the pattern of staining was notably different. Both age groups showed two distinct populations of nuclei with either low or high levels of mH2A, with relatively few nuclei falling in between, giving rise to biphasic histogram distributions (Fig. 6B). Interestingly, the proportion of nuclei in the low and high expression groups changed with age, with an increased fraction of cells displaying higher levels of mH2A in the old animals (Fig. 6C). Higher levels of mH2A in old animals were also confirmed by immunoblotting (data not shown).

Expression of heterochromatic marks in primate tissues

Having obtained evidence for increased age-associated heterochromatinization in several murine tissues, we asked whether

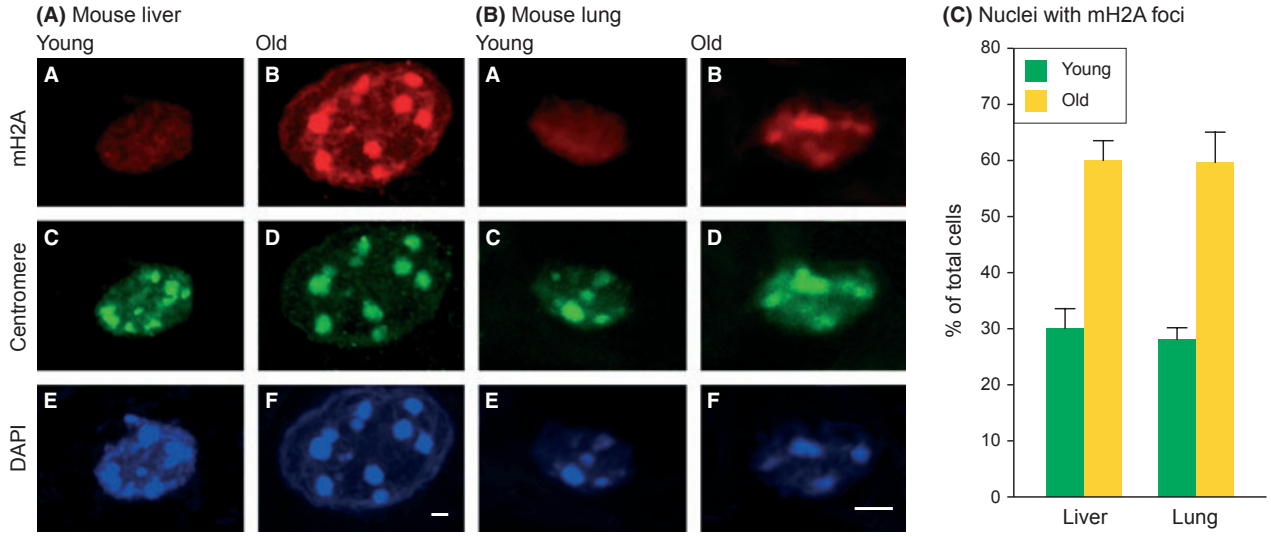

Fig. 5 Association of histone macroH2A (mH2A) with pericentromeric heterochromatin. Representative images of single nuclei are shown at high magnification for (A) mouse liver and (B) mouse lung. Panels show the same nucleus stained for mH2A (top row, A, B), centromeres (middle row, C, D), and DAPI (bottom row, E, F). A young nucleus is shown on the left (A, C, E), and an old nucleus on the right (B, D, F). Scale bars designate 2 μm. Note that lung nuclei are considerably smaller than liver nuclei and are shown at higher magnification. (C) Quantification of mH2A-staining pericentromeric foci. A cell was considered positive if it displayed at least one mH2A focus colocalizing with a DAPI focus. At least 200 nuclei were scored for each condition. Error bars indicate the SEM.

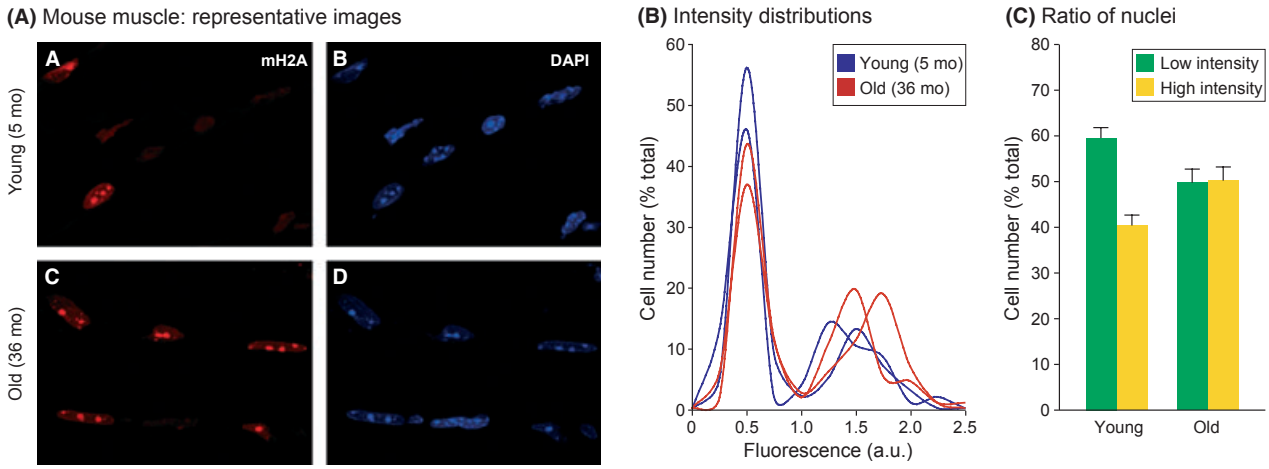

Fig. 6 Quantitative single cell measurements of histone macroH2A (mH2A) protein levels in mouse skeletal muscle. (A) Representative images of sections from 5- and 36-month-old male quadriceps muscle. The bright foci in the DAPI images are the prominent pericentromeric heterochromatin found in this species. (B) Immunofluorescent images collected in the experiment shown in panel A were quantified as indicated in Experimental procedures, expressed as ratios of mH2A and DAPI intensities for each nucleus, and plotted as histograms of cell number (% of total) against fluorescence intensity in arbitrary units (a.u.). Representative histograms for two young (blue) and two old (red) animals are shown. Note the prominent biphasic profile of the histograms. (C) Quantification of mH2A levels detected by immunofluorescence. The number of cells (% of total) under the low (green) and high (yellow) intensity peaks were calculated for each histogram, and mean values were calculated for the young and old age groups. A total of five young and five old animals were included in the analysis. Error bars indicate the SEM. The ratio of low to high intensity cells was 1.48 for the young animals, and 0.99 for the old animals. The difference between the ratios of low and high intensity cells is significant at $P = 0.0080$ calculated using a two-tailed student's test. The experiment was repeated three times with consistent results.

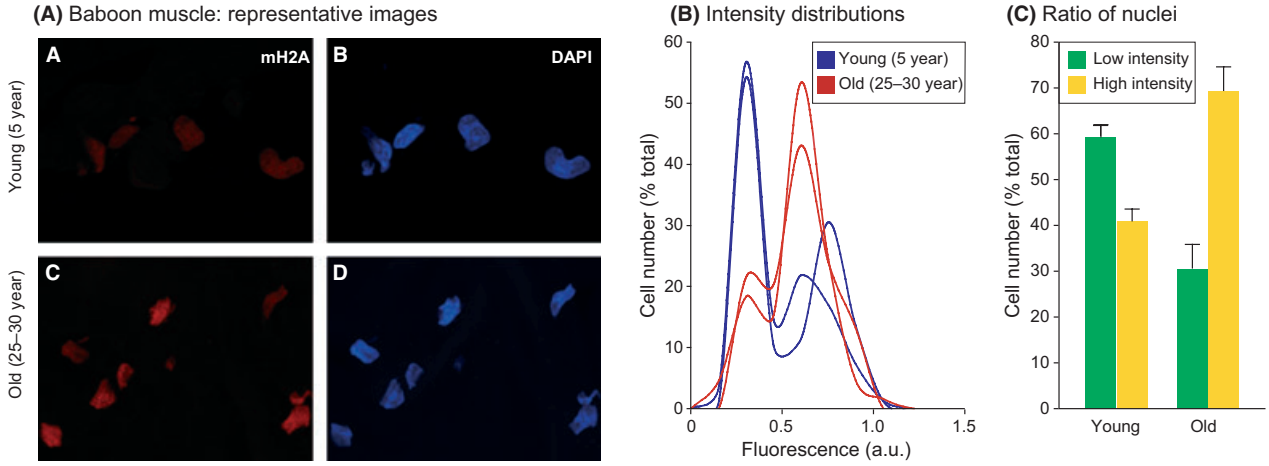

Fig. 7 Quantitative single cell measurements of histone macroH2A (mH2A) protein levels in baboon skeletal muscle. (A) Representative images of sections from 5-year-old and 25- to 30-year-old vastus lateralis muscle. Animals of both sexes were included. (B) Immunofluorescent images collected in the experiment shown in panel A were quantified as indicated in Experimental procedures, expressed as ratios of mH2A and DAPI intensities for each nucleus, and plotted as histograms of cell number (% of total) against fluorescence intensity in arbitrary units (a.u.). Representative histograms for two young (blue) and two old (red) animals are shown. Note the prominent biphasic profile of the histograms. (C) Quantification of mH2A levels detected by immunofluorescence. The number of cells (% of total) under the low (green) and high (yellow) intensity peaks was calculated for each histogram, and mean values were calculated for the young and old age groups. A total of five young and six old animals were included in the analysis. Error bars indicate the SEM. The ratio of low to high intensity cells was 1.45 for the young animals, and 0.44 for the old animals. The difference between the ratios of low- and high-intensity cells is significant at $P = 0.0018$ calculated using a two-tailed student's test. The experiment was repeated three times with consistent results.

similar trends also occur in other species. As we have previously collected skin and skeletal muscle biopsies from baboons of varying ages (Herbig *et al.*, 2006; Jeyapalan *et al.*, 2007), we applied our new single cell heterochromatinization assay to these specimens. Examination of baboon skeletal muscle revealed strong age-associated trends (Fig. 7A). As was the case with murine skeletal muscle, the distributions were clearly biphasic with distinct high- and low-intensity nuclei (Fig. 7B). Furthermore, the shift in the ratio from low- to high-intensity nuclei was very pronounced, changing more than threefold from 1.45 in the young animals to 0.44 in the old animals (Fig. 7C).

In contrast, analysis of dermal fibroblasts in skin biopsies revealed a more subtle increase in mH2A levels (Fig. S4). Many

but not all of the specimens showed a biphasic profile. The overall mean intensity in the old specimens increased, but fell just below statistical significance ($P = 0.065$). The most likely explanation is that the skin is subject to environmental exposure, which could obscure an underlying age-associated pattern. We noted that the young animals had particularly heterogeneous distributions, but unfortunately, we did not have access to additional animals to explore this phenomenon further.

Discussion

HP1 was first described as a heterochromatin-associated protein required for heterochromatin-induced gene silencing during position effect variegation in *Drosophila* (Eissenberg & Elgin, 2000). HP1 proteins are highly conserved in evolution, and are enriched in constitutive heterochromatin in centromeric regions, telomeres, and silenced interspersed repetitive elements, as well as in regions of facultative heterochromatin (Kwon & Workman, 2008). HP1 proteins bind to the H3K9Me3 mark and are believed to play an active role in cross-linking the associated nucleosomes into higher-order chromatin structures that represent the characteristic hallmark of heterochromatin (Jenuwein & Allis, 2001); recently additional roles, such as in DNA repair, have been described (Timinszky *et al.*, 2009; Billur *et al.*, 2010; Teschendorff *et al.*, 2010). The histone variant mH2A is highly conserved in vertebrates but absent in most invertebrates (Changolkar *et al.*, 2008). It is enriched in constitutive heterochromatin (such as some interspersed repetitive elements and pericentromeric regions), facultative heterochromatin (such as the inactive X chromosome in female cells), and depleted on active genes (Changolkar & Pehrson, 2006; Choo *et al.*, 2006, 2007; Changolkar *et al.*, 2010). The mH2A nonhistone domain has been reported to antagonize transcription initiation by blocking histone acetylation and interfering with nucleosome remodeling (Doyen *et al.*, 2006). HP1β co-purifies with mH2A-containing chromatin fragments (Changolkar & Pehrson, 2006), and both proteins have been colocalized in SAHF (Narita *et al.*, 2003; Zhang *et al.*, 2005). We found that the levels of mH2A and HP1β increase in parallel in individual HDF nuclei as they approach replicative senescence. At the single-cell level, these proteins therefore represent ideal markers of heterochromatin.

Our work was stimulated by the desire to use SAHF, a promising new marker of cellular senescence, to assess the existence and prevalence of senescent cells *in vivo*. Based on the studies reported here, we believe that it is reasonable to conclude that SAHF do not accumulate with aging *in vivo*, at least as morphologically distinct structures that can be visualized by microscopy in mouse or baboon. Recently, we found that mouse fibroblasts undergoing senescence in culture do not form robust SAHF, although they do display elevated mH2A levels (Kennedy *et al.*, 2010). But do the increased levels of mH2A that are clearly demonstrable *in vivo* represent senescent cells? Several lines of evidence suggest that this is unlikely to be the whole story. First, other markers of senescence report relatively few senescent cells, compared with the frequencies of cells we observe with increased heterochromatin markers. When stained for the senescence-associated β-galactosidase (SA-β-Gal) marker, the tissues examined here (lung, liver, dermis, skeletal muscle) show positive cells in the range of 2–5% (Dimri *et al.*, 1995; Wang *et al.*, 2009) (our data). While good correlations between SA-β-Gal-positive and senescent cells have been reported *in vitro* (Itahana *et al.*, 2003; Passos *et al.*, 2007), the assay is much less reliable in tissue sections, which can lead to underestimation of senescent cells (Itahana *et al.*, 2007). Another method to determine the frequency of senescent cells is to score cells that stain positive for DNA damage foci-associated proteins γ-H2AX or 53BP1 (Bartkova *et al.*, 2006; Di Micco *et al.*, 2006; Herbig *et al.*, 2006; Jeyapalan *et al.*, 2007; Sedelnikova *et al.*, 2008; Wang *et al.*, 2009; Le *et al.*, 2010). This approach is gaining popularity because of recent evidence that many, if not all, senescent states may be caused (or accompanied) by features of genotoxic stress and a DNA damage response (DDR) (d'Adda di Fagagna, 2008). These methods are, however, likely to overestimate the frequencies of senescent cells, because some cells that sustain DNA damage will in all likelihood be repaired, while others may enter alternate pathways, such as apoptosis. Wang *et al.* (2009) reported frequencies of DNA damage foci in the lung, liver and skeletal muscle of 6.7%, 8.4% and 0.3% in young mice, and 19%, 17% and 1.5% in old animals, respectively. In contrast, we observe in old animals 60–100% of the cells (depending on the tissue) to display elevated mH2A levels.

In the mouse lung, we observed an approximately 1.8-fold increase in mH2A levels, characterized by monophasic expression histograms at both ages and a shift in peak intensity at old age (Fig. 4). Our samples were obtained from the alveolar region of the lung, which is composed of predominantly four cell types: type I and type II epithelial cells, endothelial cells, and fibroblasts. The absence of distinct subpopulations in our immunofluorescence data (which would appear as shoulders or multiple peaks in the histograms) indicate that all cell types are affected by increased mH2A levels, although it remains possible that some cell types may be affected more than others. This widespread response appears to be distinct from the discrete cohort of 19% DDR-positive cells reported in aged mouse lung (Wang *et al.*, 2009). In our study, the frequency of DDR-positive cells was in the range of 10% in old animals; these lower numbers may reflect the fact that Wang *et al.* used extremely old (42 month C57Bl⁄6) animals. Thus, while it is possible that DDR-positive cells comprise a subset of cells with high mH2A levels, it is also evident that the majority of normal cells in the lung without any evidence of DDR display elevated mH2A levels with age. While the DDR-positive cells may be senescent, we consider it unlikely that all of the mH2A-positive cells are senescent.

In the skeletal muscle, we observed two populations of cells with either low or high mH2A levels, which were clearly evident as distinct peaks in the immunofluorescence histograms. The pattern of expression was very similar in mouse and baboon. A significant number of nuclei (approximately 40% in both mouse and baboon) displayed high mH2A levels even in young animals. However, there was a clear increase in the proportion of nuclei

with high mH2A levels in older animals. An overall increase in mH2A levels was also observed by immunoblotting. Skeletal muscle tissue is comprised of predominantly one cell type, the fully differentiated postmitotic myocyte. As normal healthy myocytes have very long chronologic lifespans, turnover occurs at exceedingly low rates under nonpathologic conditions. Cellular senescence, given its canonical definition as a premature or inappropriate replicative arrest, does not affect differentiated postmitotic tissues, and muscle is thus not believed to age replicatively, although it is obviously susceptible to chronologic aging. Accordingly, mouse skeletal muscle contains very few SA-β-Gal-positive cells (< 1%) and their frequency does not increase with age (our observations). Evaluating other markers of cellular senescence, we observed very low levels (< 2%) of cells with telomeric damage, and their number did not increase with age in the baboon (Jeyapalan *et al.*, 2007). Similarly, mouse muscle shows very low frequencies of DDR-positive cells, which do not increase with age (Wang *et al.*, 2009), a finding that we confirmed in baboon muscle (Jeyapalan *et al.*, 2007). In relation to most other tissues examined, skeletal muscle also displays very marginal age-associated upregulation of p16 (Edwards *et al.*, 2007), another important marker of senescence (Krishnamurthy *et al.*, 2004). It is thus unlikely that the mature myocytes with high mH2A levels are senescent, at least using our current definitions and understanding of cellular senescence. Given the strong association of mH2A with heterochromatinization, it will be of great interest to investigate the epigenetic basis of the many gene expression changes known to occur in muscle with aging.

In the liver, while we saw an overall increase in mH2A levels, this was obscured by the polyploidization that occurs with age in this tissue, so the ratios of mH2A to DAPI did not change much. The prominent pericentromeric heterochromatin found in these cells allowed us, however, to detect a clear increase in mH2A localization to this compartment, a finding that we subsequently extended to lung and skeletal muscle tissue [very similar findings have been recently reported in mouse liver using an antibody to H3K9Me3 (Jin *et al.*, 2010)]. It thus appears that the additional mH2A in old cells is targeted, at least in part, to constitutive heterochromatin, although this does not account for the overall increase, and higher signal is evident throughout the nucleus.

The age-associated increase in heterochromatin marks documented here and in other recent studies (Sarg *et al.*, 2002; Jin *et al.*, 2010; Wood *et al.*, 2010) contrasts with the well-documented decrease in DNA methylation (Sedivy *et al.*, 2008; Calvanese *et al.*, 2009). Although the reason for this discrepancy remains to be explored, it is tempting to speculate that it reflects a progressive, age-associated disorganization of chromatin, which may be an unavoidable consequence of its inherently dynamic nature. A recent report (Wood *et al.*, 2010) used chromatin immunoprecipitation (ChIP) and whole genome tiling arrays in *Drosophila* to document that transcription-activating histone modifications associated with genes and exonic regions decreased with age, while repressive marks became dispersed throughout the genome, showing relative decreases over heterochromatic regions and increases over euchromatic regions. Together, these results are consistent with our findings and indicative of an increase in transcriptionally repressive heterochromatin, particularly at gene coding regions. Of relevance to our findings, the levels of H3K9Me3 and HP1 increased with age, hinting at strong conservation in these processes.

We still know very little about the epigenetics of aging, but it is rapidly coming to light that chromatin is subject to profound age-associated changes (Fraga *et al.*, 2005). In this communication, we describe the development of an assay, based on immunofluorescence microscopy, capable of quantitatively detecting, at the single-cell level, changes in the nuclear content of chromatin-associated proteins. We use the assay to demonstrate increased levels of the heterochromatin-associated proteins mH2A and HP1β in human fibroblasts during replicative senescence in culture, and for the first time, an age-associated increase in these heterochromatin marks in several tissues of mice and primates. The assay has undergone extensive development and validation by immunoblotting, and is capable of accurately assessing differences of 1.5-fold (and even lower if sufficiently large numbers of cells are scored). As is the case for any immunofluorescence-based assay, it can be limited by the availability of antibodies of adequate affinity and limited cross-reactivity. Here we have focused on mH2A and HP1β, two known constituents of heterochromatin against which we were able to locate very good antibodies, but the principles of the assay are generalizable to any nuclear antigen of interest. The advantage of this approach over biochemical methods is the ability to visualize individual cells in nondisaggregated tissue, providing quantitative single-cell level information on chromatin states in different cell types, morphologic structures, or regions of tissue pathology. Another important advantage is the small amount of biologic material that is needed (at the limit, a handful of 6–8 μm tissue sections) allowing the examination of microscopic structures, such as stem cells in their native niches, or limited and valuable archival material. Monitoring of histone modifications would be of particular interest, and we have been recently able to obtain quantitative information on H3K9Me3 and H3K27Me3.

Experimental procedures

Cell culture

Human embryonic lung fibroblasts, strain LF1 (Herbig *et al.*, 2004), were cultured in Ham's F10 nutrient mixture (Invitrogen, Carlsbad, CA, USA) supplemented with 15% fetal bovine serum (Hyclone, Logan, UT, USA), 20 mM L-glutamine and penicillin/streptomycin (Sigma-Aldrich, St. Louis, MO, USA). Cultures were maintained using a 1:4 subculture regimen and incubated at 37 °C in an atmosphere of 92.5% N_2, 5%CO_2, and 2.5% O_2. Cells were split into fresh medium after reaching 80% confluence. For immunofluorescence, cells were plated onto glass coverslips and grown to 80% confluence.

Tissue specimens

Mouse tissues of strain C57BL/6 were obtained from the National Institute on Aging (NIA) Aged Rodent Tissue Bank (http://www.nia.nih.gov/ResearchInformation/ScientificResources/AgedRodentTissueBankHandbook/), or collected in-house from mice obtained from the NIA Aged Rodent Colonies (http://www.nia.nih.gov/ResearchInformation/ScientificResources/AgedRodentColoniesHandbook/). Baboon skin and muscle tissues were obtained from the Southwest Foundation for Biomedical Research (San Antonio, TX, USA). Biopsy procedures have been previously described (Herbig *et al.*, 2006; Jeyapalan *et al.*, 2007). All tissues were embedded in Tissue-Tek optimal temperature cutting compound (OCT; Sakura Finetek, USA , Torrance, CA, USA) at the time of harvest and stored at −80 °C. Eight-micrometer-tissue sections were cut using a cryomicrotome (Leica CM3050S, Leica Mircrosystems, Wetzlar, Germany) at −29 °C for mouse lung, −19 °C for mouse liver, −23 °C for mouse muscle and baboon muscle, and −28 °C for baboon skin.

Quantitative immunofluorescence

For fixation of cells, 4% paraformaldehyde in phosphate-buffered saline (PBS, pH 7.4), precooled to 4 °C, was added to the samples and incubated for 20 min at room temperature. Permeablization was with 0.2% Triton X-100 in PBS for 20 min at room temperature. For fixation of tissues, 4% paraformaldehyde and 0.5% Triton X-100 in PBS, prewarmed to 37 °C, were added to the samples and incubated for 20 min at room temperature. No further permeabilization was performed. For both sample types, nonspecific binding was blocked by incubation in 4% bovine serum albumin (BSA; fraction V, Thermo Fisher Scientific, Waltham, MA, USA), 2% donkey serum, and 0.1% Triton X-100 in PBS for 1 h at room temperature. Antibodies were diluted in the above blocking solution at saturating concentrations (Table S1) and incubated for 2 h at room temperature (cells) or overnight at 4 °C (tissue) with rocking in a humidified chamber. Secondary antibodies, when used, were also diluted in blocking solution and incubated for 2 h at room temperature. Nuclei were counterstained with 2 μg mL^{-1} DAPI in PBS, containing 0.2% Triton X-100 for 15 min (cells) or 45 min (tissues).

Cell culture images were acquired using a Zeiss Axiovert 200M (Carl Zeiss AG, Oberkochen, Germany) fluorescence microscope equipped with a Roper CoolSnap HQ monochrome camera controlled by MetaMorph software (Molecular Devices, Downingtown, PA, USA). Tissue sections were imaged on a Zeiss LSM 710 Confocal Laser Scanning Microscope. A z-series encompassing the full thickness of the tissue was collected for each field. All microscope settings and exposure times were set to collect images below saturation and were kept constant for all images taken in one experiment. Image analysis was performed using either MetaMorph software or ImageJ open source software from the NIH (http://rsbweb.nih.gov/ij/). The region of each nucleus in an image was defined using the DAPI channel (435–485 nm emission), and the total and average fluorescence intensities within this region were recorded for all of the fluorophores used (depending on the experiment): DAPI, Cy3 (590–650 nm emission) and Cy5 or Alexa 647 (665 nm long pass emission). To automate the analysis, ImageJ macros were developed and are available at upon request. For each sample, a total of 100–500 nuclei were recorded in multiple fields. For cell culture images, mH2A and HP1β levels were expressed as average intensities in arbitrary fluorescence units (a.u.). For tissue images, mH2A fluorescence intensities were normalized to DAPI intensities for each nucleus. Nuclei were distributed into bins based on their expression levels, and plotted as histograms with the value of each bin shown as % of total nuclei.

Quantitative immunoblotting

Cells were harvested by scraping into PBS, collected by centrifugation and aliquots were counted in a hemocytometer. Cells were lysed in approximately 10 pellet volumes of sample buffer (60 mM Tris, pH 6.8, 2% SDS, 10% glycerol, 100 mM DTT) and boiled for 5 min. Whole cell extracts equivalent to 1×10^5 starting cells per lane were separated by SDS-PAGE and transferred onto Immobilon-P membranes (Millipore, Billerica, MA, USA). Signals were detected using the LI-COR Odyssey (LI-COR Biosciences, Lincoln, NE, USA) infrared imaging system, and analyzed with the gel analysis component of ImageJ software.

Antibodies

Rabbit polyclonal antibodies against human mH2A1.1 and mH2A1.2 were raised in the Fox Chase Cancer Center Laboratory Animal Facility (Zhang *et al.*, 2007). The antigens used were purified GST fusion proteins containing the entire nonhistone domains of mH2A1.1 and mH2A1.2. While the two proteins differ by one alternatively spliced exon (29 and 32 amino acids in mH2A1.1 and 1.2, respectively), the remaining 179 residues are in common. Not surprisingly, the resulting antisera react with both the mH2A1.1 and mH2A1.2 proteins. The independently raised mH2A1.1 and mH2A1.2 antibodies behaved equivalently in all the assays presented in this communication. In immunoblots, both antibodies visualize a single major band for mH2A1.1 or mH2A1.2, depending on the tissue. Prior to use in our studies, the antibodies were affinity purified on columns with immobilized fusion proteins. Where indicated, the antibodies were directly labeled with Alexa Fluor 647 using the monoclonal antibody labeling kit A20186 from Invitrogen. Control immunofluorescence experiments using mH2A1 knockout mouse MEF and tissues to assess nonspecific background are shown in Fig. S5. Antibodies against HP1β (MAB3448) were from Millipore. Human anti-centromere autoantibody (Cat. No. 15-235) was purchased from Antibodies Incorporated. For immunofluorescence, Cy3- and Cy5-labeled secondary antibodies were obtained from Jackson ImmunoResearch. For immuno-

blotting, in addition to the above indicated antibodies to mH2A and HP1β, primary antibodies to p16 (sc-56330, Santa Cruz) and p21 (sc-397, Santa Cruz) were used. Secondary antibodies for immunoblotting were labeled with Odyssey IRDye 800CW (LI-COR Biosciences, 926-32210 and 926-32211) and with Alexa Fluor 680 (Invitrogen, A21058 and A21109.

Acknowledgments

The microscopic analysis presented in this work was performed in the Leduc Bioimaging Facility at Brown University, and we gratefully acknowledge the generous and skilled support of its staff. We are greatly indebted to John R. Pehrson and his laboratory members (especially Adrian Leu) at the University of Pennsylvania for providing MEF and tissues from mH2A1 knockout mice on very short notice. This work was supported by NIH/NIA grant R37 AG016694 to J.M.S. J.A.K. was supported in part by NIH/NCRR P20 RR015578-10S1. The Genomics Core Facility in the Laboratories for Molecular Medicine at Brown University was supported in part by the COBRE award from the NIH/NCRR P20 RR015578. P.D.A. was supported by grant P01 AG031862 from the NIH/NIA and by grant BB/H021019/1 from the BBSRC. J.M.S. is a Senior Scholar of the Ellison Medical Foundation.

Author contributions

J.M.S. and J.A.K designed the experiments and guided their execution. J.A.K., M.T.-A., A.N.S., J.C.J., U. M.-N., A.L.P, J.M. and E.S.R. performed the experiments. J.M.S. and J.A.K. wrote the manuscript. P.D.A. provided antibodies to mH2A, helpful guidance throughout this work, and participated in the writing of the manuscript.

References

Adams PD (2009) Healing and hurting: molecular mechanisms, functions, and pathologies of cellular senescence. *Mol. Cell* **36**, 2–14.

d'Adda di Fagagna F (2008) Living on a break: cellular senescence as a DNA-damage response. *Nat. Rev. Cancer* **8**, 512–522.

Bahar R, Hartmann CH, Rodriguez KA, Denny AD, Busuttil RA, Dolle ME, Calder RB, Chisholm GB, Pollock BH, Klein CA, Vijg J (2006) Increased cell-to-cell variation in gene expression in ageing mouse heart. *Nature* **441**, 1011–1014.

Bartkova J, Rezaei N, Liontos M, Karakaidos P, Kletsas D, Issaeva N, Vassiliou LV, Kolettas E, Niforou K, Zoumpourlis VC, Takaoka M, Nakagawa H, Tort F, Fugger K, Johansson F, Sehested M, Andersen CL, Dyrskjot L, Orntoft T, Lukas J, Kittas C, Helleday T, Halazonetis TD, Bartek J, Gorgoulis VG (2006) Oncogene-induced senescence is part of the tumorigenesis barrier imposed by DNA damage checkpoints. *Nature* **444**, 633–637.

Berger SL (2007) The complex language of chromatin regulation during transcription. *Nature* **447**, 407–412.

Billur M, Bartunik HD, Singh PB (2010) The essential function of HP1 beta: a case of the tail wagging the dog? *Trends Biochem. Sci.* **35**, 115–123.

Bodnar AG, Ouellette M, Frolkis M, Holt SE, Chiu CP, Morin GB, Harley CB, Shay JW, Lichtsteiner S, Wright WE (1998) Extension of life-span by introduction of telomerase into normal human cells. *Science* **279**, 349–352.

Bollati V, Schwartz J, Wright R, Litonjua A, Tarantini L, Suh H, Sparrow D, Vokonas P, Baccarelli A (2009) Decline in genomic DNA methylation through aging in a cohort of elderly subjects. *Mech. Ageing Dev.* **130**, 234–239.

Bork S, Pfister S, Witt H, Horn P, Korn B, Ho AD, Wagner W (2010) DNA methylation pattern changes upon long-term culture and aging of human mesenchymal stromal cells. *Aging Cell* **9**, 54–63.

Calvanese V, Lara E, Kahn A, Fraga MF (2009) The role of epigenetics in aging and age-related diseases. *Ageing Res. Rev.* **8**, 268–276.

Changolkar LN, Pehrson JR (2006) macroH2A1 histone variants are depleted on active genes but concentrated on the inactive X chromosome. *Mol. Cell. Biol.* **26**, 4410–4420.

Changolkar LN, Singh G, Pehrson JR (2008) macroH2A1-dependent silencing of endogenous murine leukemia viruses. *Mol. Cell. Biol.* **28**, 2059–2065.

Changolkar LN, Singh G, Cui K, Berletch JB, Zhao K, Disteche CM, Pehrson JR (2010) Genome-wide distribution of macroH2A1 histone variants in mouse liver chromatin. *Mol. Cell. Biol.* **30**, 5473–5483.

Choo JH, Kim JD, Chung JH, Stubbs L, Kim J (2006) Allele-specific deposition of macroH2A1 in imprinting control regions. *Hum. Mol. Genet.* **15**, 717–724.

Choo JH, Kim JD, Kim J (2007) MacroH2A1 knockdown effects on the Peg3 imprinted domain. *BMC Genomics* **8**, 479.

Collado M, Blasco MA, Serrano M (2007) Cellular senescence in cancer and aging. *Cell* **130**, 223–233.

Cristofalo VJ, Pignolo RJ (1993) Replicative senescence of human fibroblast-like cells in culture. *Physiol. Rev.* **73**, 617–638.

Di Micco R, Fumagalli M, Cicalese A, Piccinin S, Gasparini P, Luise C, Schurra C, Garre M, Nuciforo PG, Bensimon A, Maestro R, Pelicci PG, d'Adda di Fagagna F (2006) Oncogene-induced senescence is a DNA damage response triggered by DNA hyper-replication. *Nature* **444**, 638–642.

Dimri GP, Lee X, Basile G, Acosta M, Scott G, Roskelley C, Medrano EE, Linskens M, Rubelj I, Pereira-Smith O, Peacocke M, Campisi J (1995) A biomarker that identifies senescent human cells in culture and in aging skin in vivo. *Proc. Natl Acad. Sci. USA* **92**, 9363–9367.

Doyen CM, An W, Angelov D, Bondarenko V, Mietton F, Studitsky VM, Hamiche A, Roeder RG, Bouvet P, Dimitrov S (2006) Mechanism of polymerase II transcription repression by the histone variant macroH2A. *Mol. Cell. Biol.* **26**, 1156–1164.

Edwards MG, Anderson RM, Yuan M, Kendziorski CM, Weindruch R, Prolla TA (2007) Gene expression profiling of aging reveals activation of a p53-mediated transcriptional program. *BMC Genomics* **8**, 80.

Eissenberg JC, Elgin SC (2000) The HP1 protein family: getting a grip on chromatin. *Curr. Opin. Genet. Dev.* **10**, 204–210.

Fraga MF, Ballestar E, Paz MF, Ropero S, Setien F, Ballestar ML, Heine-Suner D, Cigudosa JC, Urioste M, Benitez J, Boix-Chornet M, Sanchez-Aguilera A, Ling C, Carlsson E, Poulsen P, Vaag A, Stephan Z, Spector TD, Wu YZ, Plass C, Esteller M (2005) Epigenetic differences arise during the lifetime of monozygotic twins. *Proc. Natl Acad. Sci. USA* **102**, 10604–10609.

Funayama R, Saito M, Tanobe H, Ishikawa F (2006) Loss of linker histone H1 in cellular senescence. *J. Cell Biol.* **175**, 869–880.

Grewal SI, Jia S (2007) Heterochromatin revisited. *Nat. Rev. Genet.* **8**, 35–46.

Hayflick L, Moorhead PS (1961) The serial cultivation of human diploid cell strains. *Exp. Cell Res.* **25**, 585–621.

Herbig U, Jobling WA, Chen BP, Chen DJ, Sedivy JM (2004) Telomere shortening triggers senescence of human cells through a pathway involving ATM, p53, and p21(CIP1), but not p16(INK4a). *Mol. Cell* **14**, 501–513.

Herbig U, Ferreira M, Condel L, Carey D, Sedivy JM (2006) Cellular senescence in aging primates. *Science* **311**, 1257.

Itahana K, Zou Y, Itahana Y, Martinez JL, Beausejour C, Jacobs JJ, Van Lohuizen M, Band V, Campisi J, Dimri GP (2003) Control of the replicative life span of human fibroblasts by p16 and the polycomb protein Bmi-1. *Mol. Cell. Biol.* **23**, 389–401.

Itahana K, Campisi J, Dimri GP (2007) Methods to detect biomarkers of cellular senescence: the senescence-associated beta-galactosidase assay. *Methods Mol. Biol.* **371**, 21–31.

Jenuwein T, Allis CD (2001) Translating the histone code. *Science* **293**, 1074–1080.

Jeyapalan JC, Ferreira M, Sedivy JM, Herbig U (2007) Accumulation of senescent cells in mitotic tissue of aging primates. *Mech. Ageing Dev.* **128**, 36–44.

Jin J, Wang GL, Iakova P, Shi X, Haeflinger S, Finegold M, Timchenko NA (2010) Epigenetic changes play critical role in age-associated dysfunctions of the liver. *Aging Cell*, **9**, 895–910.

Jintaridth P, Mutirangura A (2010) Distinctive patterns of age-dependent hypomethylation in interspersed repetitive sequences. *Physiol. Genomics* **41**, 194–200.

Kennedy BK, Gotta M, Sinclair DA, Mills K, McNabb DS, Murthy M, Pak SM, Laroche T, Gasser SM, Guarente L (1997) Redistribution of silencing proteins from telomeres to the nucleolus is associated with extension of life span in S. cerevisiae. *Cell* **89**, 381–391.

Kennedy AL, McBryan T, Enders GH, Johnson FB, Zhang R, Adams PD (2010) Senescent mouse cells fail to overtly regulate the HIRA histone chaperone and do not form robust Senescence Associated Heterochromatin Foci. *Cell Div.* **5**, 16.

Krishnamurthy J, Torrice C, Ramsey MR, Kovalev GI, Al-Regaiey K, Su L, Sharpless NE (2004) Ink4a/Arf expression is a biomarker of aging. *J. Clin. Invest.* **114**, 1299–1307.

Kwon SH, Workman JL (2008) The heterochromatin protein 1 (HP1) family: put away a bias toward HP1. *Mol. Cells* **26**, 217–227.

Le ON, Rodier F, Fontaine F, Coppe JP, Campisi J, DeGregori J, Laverdiere C, Kokta V, Haddad E, Beausejour CM (2010) Ionizing radiation-induced long-term expression of senescence markers in mice is independent of p53 and immune status. *Aging Cell* **9**, 398–409.

Narita M, Nunez S, Heard E, Narita M, Lin AW, Hearn SA, Spector DL, Hannon GJ, Lowe SW (2003) Rb-mediated heterochromatin formation and silencing of E2F target genes during cellular senescence. *Cell* **113**, 703–716.

Narita M, Narita M, Krizhanovsky V, Nunez S, Chicas A, Hearn SA, Myers MP, Lowe SW (2006) A novel role for high-mobility group a proteins in cellular senescence and heterochromatin formation. *Cell* **126**, 503–514.

Oberdoerffer P, Sinclair DA (2007) The role of nuclear architecture in genomic instability and ageing. *Nat. Rev. Mol. Cell Biol.* **8**, 692–702.

Oberdoerffer P, Michan S, McVay M, Mostoslavsky R, Vann J, Park SK, Hartlerode A, Stegmuller J, Hafner A, Loerch P, Wright SM, Mills KD, Bonni A, Yankner BA, Scully R, Prolla TA, Alt FW, Sinclair DA (2008) SIRT1 redistribution on chromatin promotes genomic stability but alters gene expression during aging. *Cell* **135**, 907–918.

Passos JF, Saretzki G, Ahmed S, Nelson G, Richter T, Peters H, Wappler I, Birket MJ, Harold G, Schaeuble K, Birch-Machin MA, Kirkwood TB, von Zglinicki T (2007) Mitochondrial dysfunction accounts for the stochastic heterogeneity in telomere-dependent senescence. *PLoS Biol.* **5**, e110.

Prieur A, Peeper DS (2008) Cellular senescence in vivo: a barrier to tumorigenesis. *Curr. Opin. Cell Biol.* **20**, 150–155.

Rakyan VK, Down TA, Maslau S, Andrew T, Yang TP, Beyan H, Whittaker P, McCann OT, Finer S, Valdes AM, Leslie RD, Deloukas P, Spector TD (2010) Human aging-associated DNA hypermethylation occurs preferentially at bivalent chromatin domains. *Genome Res.* **20**, 434–439.

Sarg B, Koutzamani E, Helliger W, Rundquist I, Lindner HH (2002) Postsynthetic trimethylation of histone H4 at lysine 20 in mammalian tissues is associated with aging. *J. Biol. Chem.* **277**, 39195–39201.

Sedelnikova OA, Horikawa I, Redon C, Nakamura A, Zimonjic DB, Popescu NC, Bonner WM (2008) Delayed kinetics of DNA double-strand break processing in normal and pathological aging. *Aging Cell* **7**, 89–100.

Sedivy JM, Munoz-Najar UM, Jeyapalan JC, Campisi J (2007) Cellular senescence: a link between tumor suppression and organismal aging?In *The Molecular Biology of Aging*. (Guarente L, Partridge L, eds). Cold Spring Harbor, NY: Cold Spring Harbor Laboratory Press, pp. 185–214.

Sedivy JM, Banumathy G, Adams PD (2008) Aging by epigenetics – a consequence of chromatin damage? *Exp. Cell Res.* **314**, 1909–1917.

Simon JA, Kingston RE (2009) Mechanisms of polycomb gene silencing: knowns and unknowns. *Nat. Rev. Mol. Cell Biol.* **10**, 697–708.

Talbert PB, Henikoff S (2006) Spreading of silent chromatin: inaction at a distance. *Nat. Rev. Genet.* **7**, 793–803.

Teschendorff AE, Menon U, Gentry-Maharaj A, Ramus SJ, Weisenberger DJ, Shen H, Campan M, Noushmehr H, Bell CG, Maxwell AP, Savage DA, Mueller-Holzner E, Marth C, Kocjan G, Gayther SA, Jones A, Beck S, Wagner W, Laird PW, Jacobs IJ, Widschwendter M (2010) Age-dependent DNA methylation of genes that are suppressed in stem cells is a hallmark of cancer. *Genome Res.* **20**, 440–446.

Timinszky G, Till S, Hassa PO, Hothorn M, Kustatscher G, Nijmeijer B, Colombelli J, Altmeyer M, Stelzer EH, Scheffzek K, Hottiger MO, Ladurner AG (2009) A macrodomain-containing histone rearranges chromatin upon sensing PARP1 activation. *Nat. Struct. Mol. Biol.* **16**, 923–929.

Vissel B, Choo KH (1989) Mouse major (gamma) satellite DNA is highly conserved and organized into extremely long tandem arrays: implications for recombination between nonhomologous chromosomes. *Genomics* **5**, 407–414.

Wang C, Jurk D, Maddick M, Nelson G, Martin-Ruiz C, von Zglinicki T (2009) DNA damage response and cellular senescence in tissues of aging mice. *Aging Cell* **8**, 311–323.

Wilson VL, Smith RA, Ma S, Cutler RG (1987) Genomic 5-methyldeoxycytidine decreases with age. *J. Biol. Chem.* **262**, 9948–9951.

Wood JG, Hillenmeyer S, Lawrence C, Chang C, Hosier S, Lightfoot W, Mukherjee E, Jiang N, Schorl C, Brodsky AS, Neretti N, Helfand SL (2010) Chromatin remodeling in the aging genome of Drosophila. *Aging Cell*, **9**, 971–978.

Wright WE, Shay JW (2002) Historical claims and current interpretations of replicative aging. *Nat. Biotechnol.* **20**, 682–688.

Zhang R, Poustovoitov MV, Ye X, Santos HA, Chen W, Daganzo SM, Erzberger JP, Serebriiskii IG, Canutescu AA, Dunbrack RL, Pehrson JR, Berger JM, Kaufman PD, Adams PD (2005) Formation of MacroH2A-containing senescence-associated heterochromatin foci and senescence driven by ASF1a and HIRA. *Dev. Cell* **8**, 19–30.

Zhang R, Chen W, Adams PD (2007) Molecular dissection of formation of senescent associated heterochromatin foci. *Mol. Cell. Biol.* **27**, 2343–2358.

Supporting Information

Additional supporting information may be found in the online version of this article:

Fig. S1 Titration of antibody dilutions to determine saturating concentrations for quantitative signal detection.

Fig. S2 Flow cytometric analysis of the DNA content of early passage growing, quiescent, and late passage senescent HDF cells.

Fig. S3 Assessment of mH2A1 mRNA expression in HDF and murine tissues.

Fig. S4 Quantitative single cell measurements of mH2A protein levels in baboon skin.

Fig. S5 Quantitative single cell measurements of mH2A protein levels in MEF and tissues of mH2A1 knockout mice.

Table S1 Saturating concentrations of antibodies used in this study.

As a service to our authors and readers, this journal provides supporting information supplied by the authors. Such materials are peer-reviewed and may be re-organized for online delivery, but are not copy-edited or typeset. Technical support issues arising from supporting information (other than missing files) should be addressed to the authors.